International Journal of Machine Tools & Manufacture 108 (2016) 127–134

Contents lists available at ScienceDirect

International Journal of Machine Tools & Manufacture

journal homepage: www.elsevier.com/locate/ijmactool

Predicting mobile machine tool dynamics by experimental dynamic substructuring

Mohit Law [a,*], Hendrik Rentzsch [b], Steffen Ihlenfeldt [b,c]

[a] Department of Mechanical Engineering, Indian Institute of Technology, Kanpur, India
[b] Fraunhofer Institute for Machine Tools and Forming Technology IWU, Chemnitz, Germany
[c] Institute of Machine Tools and Control Engineering, Technische Universität Dresden, Germany

ARTICLE INFO

Article history:
Received 8 March 2016
Accepted 21 June 2016
Available online 22 June 2016

Keywords:
Dynamics
Mobile machine tool
Experimental substructuring
Frequency response functions

ABSTRACT

Predicting mobile machine tool dynamics prior to moving the machine to a new part and/or location is essential to guide first-time-right in situ machining solutions. This paper considers such a priori prediction of assembled dynamics under varying base/part/contact characteristics by applying dynamic substructuring procedures. Assembled dynamics are predicted by substructural coupling of the machine's known free-free response with the known response of any base/part measured at location. Since obtaining the machine's free-free response remains non-trivial, we instead extract the machine's dynamics using substructure decoupling procedures. Substructuring is carried out using measured frequency response functions. Methods are tested for robustness, and are experimentally validated.

1. Introduction

In situ machining, repair, and maintenance of large parts is made possible by moving mobile machine tools directly to the part locations. Moving the machine to the part results in significant savings in time, energy, and transportation costs that would otherwise be incurred from moving large parts to the machine's location [1,2]. An example of such a mobile machine tool developed at the Fraunhofer IWU [2,3] is shown in Fig. 1. The machine has a novel five-strut parallel kinematic configuration. A modular design allows it to be positioned at/on various parts and locations to facilitate in situ multi axis machining.

Despite its advantages, every new part and location that the machine is moved to results in different boundary conditions for the machine-part system. Varying kinematic configurations and base/part/contact characteristics significantly contribute to and influence machine dynamics. Changing dynamics interact with the cutting process and the control loop of the drives to influence and limit machining stability and accurate tracking and positioning of the tool. Since in situ machining solutions are essentially turn-key, there is a clear need for predicting the dynamics before moving the machine to the part location such as to guide selection of appropriate machining and control parameters that guarantee stable cutting and robust control.

This paper considers the experimental dynamic substructuring scheme that facilitates beforehand prediction of mobile machine tool dynamics under varying influences. Substructuring provides ways of obtaining the structural dynamics of large and/or complex structures by combining measurements and/or models of individual components/substructures for which the dynamic behavior is generally easier to determine. Substructuring hinges on being able to obtain the response of individual subsystems. Dynamics for an arbitrary part/base that the machine is moved to can be obtained by direct on site measurements. However, obtaining the machine's dynamics in its free-free configuration is non-trivial and needs special test rigs.

The main idea of this paper is to demonstrate the coupling of known dynamics of the mobile machine tool in its unsupported free-free configuration with measured dynamics of the base/part, measured separately at location for a priori prediction of the assembled system response. To obtain the machine's free-free response, we deploy substructure decoupling schemes to instead extract these dynamics from known dynamics of the mobile machine tool mounted on a calibration base, and from a priori information of the residual substructural base system. Extracted dynamics are subsequently coupled to another part/base model using the substructure coupling scheme. An overview of the proposed (de)coupling scheme is shown in Fig. 1.

Each substructural component can be represented by their spatial data, modal data, or their receptances, i.e. frequency response functions (FRFs). Spatial and modal representations form part of the family of the generalized component mode synthesis approach [4], and have been used previously in the design and analysis of machine tool concepts [5,6]. In the present case, the

* Corresponding author.
E-mail address: mlaw@iitk.ac.in (M. Law).

http://dx.doi.org/10.1016/j.ijmachtools.2016.06.006
0890-6955/

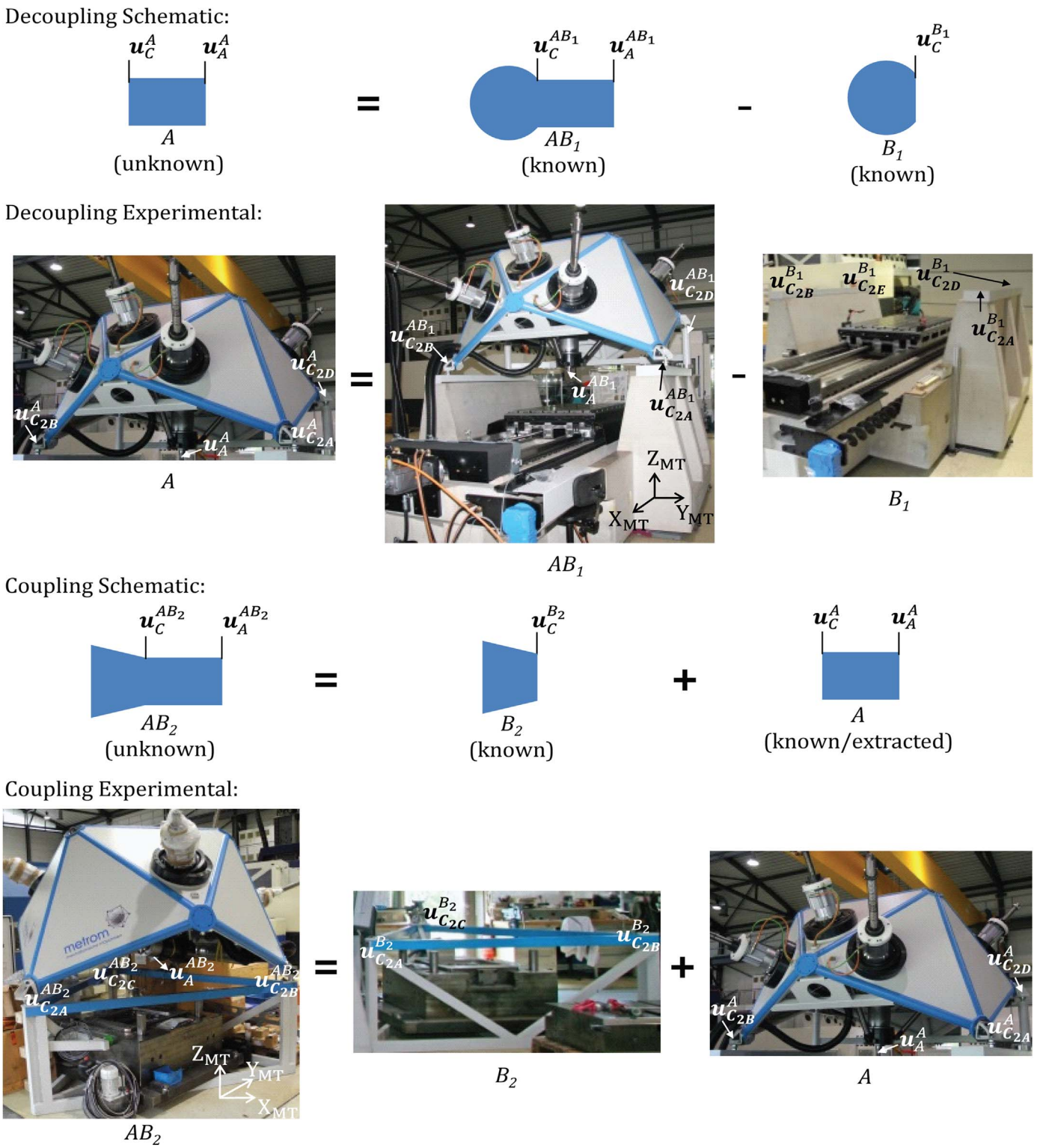

Fig. 1. Substructure decoupling and coupling schematic. AB_1 – mobile machine coupled to the first base type; B_1 – first base type only; A – extracted mobile machine tool; B_2 – second base type; AB_2 – mobile machine coupled to the second base type.

frequency based substructuring (FBS) methods [7] that instead use measured and/or modeled FRFs to describe each subsystem are preferred. FBS methods afford us the advantage of synthesizing FRFs of parts/bases measured at location with the dynamics, i.e. FRFs of the mobile machine as desired. Moreover, since tool point dynamics characterized by FRFs are directly used in predicting stable cutting conditions [8,9], predicting the assembled system dynamics using FRFs extends the utility of the methods employed in this paper.

Special cases of the FBS methods referred to as the receptance coupling substructure analysis (RCSA) approach, have found much use in machine tool applications to predict tool point dynamics [8–11]. Earlier use of RCSA/FBS methods that reported on the simple case of substructures in end-to-end contact, e.g. tool and tool-holder connections were subsequently extended in recent works for modeling complete machine tool substructures simultaneously

in contact at multiple locations [12,13]. Most of the reported work on RCSA/FBS methods was concerned with the coupling problem which combines response of subsystems to predict the assembled system response. However, sometimes the reverse problem of decoupling becomes necessary. Examples of decoupling include extraction of rotational FRFs at coupling points using the inverse RCSA techniques [9,14].

Decoupling to extract dynamics of the complete machine that are to be subsequently coupled to other substructures, as is considered in this paper, is new. Methods described in this paper build on our preliminary simulation based substructure (de)coupling work [15,16], and are thought to be novel extensions and applications of otherwise well-developed FBS methods [7,17].

Substructuring is illustrated for the example shown in Fig. 1, and the substructuring formulations are described in Section 2. The two step procedure consists of first extracting the machine response, i.e. response of subsystem A from measurements made on the machine in the assembled configuration, i.e. system AB_1, and measured dynamics of only the residual base system, i.e. subsystem B_1. In the second step, the extracted mobile machine tool response is then coupled with another subsystem B_2 to predict assembled system response AB_2. Since subsystem B_2 may represent any new part, i.e. other than B_1, that the mobile machine is moved to and mounted on, we show that it is indeed possible to couple the extracted dynamics of the mobile machine tool with measured dynamics of any base/part that can be measured at location to predict the assembled system dynamics. Experimental considerations to address issues that sometimes limit practical implementation of substructuring are discussed in Section 3, followed by validation of models in Section 4.

2. Dynamic substructuring

The mobile machine is coupled to subsystem B_1 at five locations (some of which are shown in Fig. 1), and is directly coupled to subsystem B_2 at three locations, as shown in Fig. 1. To ensure consistency in compatibility and equilibrium conditions at the interfaces during (de)coupling, the mobile machine tool dynamics (subsystem A) are extracted from AB_1 and coupled to B_2. Extracting A from AB_2 to couple with B_1 would result in underdetermined compatibility/equilibrium conditions.

Assembled system AB_1 represents the case wherein the machine is smaller and less stiff than the base/part it is mounted on, while the assembled system AB_2 represents the case wherein the mobile machine may envelope a part, and be mounted on a base/part smaller and more flexible than itself. These cases are representative of usage scenarios of the mobile machine tool.

2.1. Substructure decoupling

The decoupling problem is formulated as one of finding the behavior of subsystem A as part of the assembled system AB_1 when additional opposing forces are applied at the interfaces such that subsystem A experiences no connection forces from subsystem B_1. Assuming that dynamics of system AB_1 and subsystem B_1 are known a priori and can be measured at all locations including all coupling points, and that the dynamics are described using FRFs, a dynamic stiffness representation of the assembled system AB_1 in compact form is:

$$\boldsymbol{Z}^{AB_1}\boldsymbol{u}^{AB_1} = \boldsymbol{f}^{AB_1} - \boldsymbol{g}^{AB_1};\ \text{i.e.}$$
$$\begin{bmatrix} \boldsymbol{Z}_{AA}^{AB_1} & \boldsymbol{Z}_{AC}^{AB_1} \\ \boldsymbol{Z}_{CA}^{AB_1} & \boldsymbol{Z}_{CC}^{AB_1} \end{bmatrix} \begin{Bmatrix} \boldsymbol{u}_A^{AB_1} \\ \boldsymbol{u}_C^{AB_1} \end{Bmatrix} = \begin{Bmatrix} \boldsymbol{f}_A^{AB_1} \\ \boldsymbol{f}_C^{AB_1} \end{Bmatrix} - \begin{Bmatrix} 0 \\ \boldsymbol{g}_C^{AB_1} \end{Bmatrix} \tag{1}$$

and for subsystem B_1 is:

$$\boldsymbol{Z}^{B_1}\boldsymbol{u}_C^{B_1} = \boldsymbol{f}_C^{B_1} + \boldsymbol{g}_C^{B_1} \tag{2}$$

wherein subscripts C and A denote coupling and tool point locations respectively. Superscripts AB_1 and B_1 denote the assembled system and the subsystem respectively. $\boldsymbol{u}_A^{AB_1}$ is the vector of degrees of freedom (DoFs) corresponding to the tool point in the assembled configuration; $\boldsymbol{u}_C^{AB_1}$ is the vector of DoFs at all five coupling locations of the assembled system AB_1, i.e. $\boldsymbol{u}_C^{AB_1} = \left\{ \boldsymbol{u}_{C_{2A}}^{AB_1};\ \boldsymbol{u}_{C_{2B}}^{AB_1};\ \boldsymbol{u}_{C_{2C}}^{AB_1};\ \boldsymbol{u}_{C_{2D}}^{AB_1};\ \boldsymbol{u}_{C_{2E}}^{AB_1} \right\}^T$; $\boldsymbol{u}_C^{B_1}$ is the vector of DoFs at all of the five coupling locations of the subsystem B_1, i.e. $\boldsymbol{u}_C^{B_1} = \left\{ \boldsymbol{u}_{C_{2A}}^{B_1};\ \boldsymbol{u}_{C_{2B}}^{B_1};\ \boldsymbol{u}_{C_{2C}}^{B_1};\ \boldsymbol{u}_{C_{2D}}^{B_1};\ \boldsymbol{u}_{C_{2E}}^{B_1} \right\}^T$. $\boldsymbol{Z}$ represents the dynamic stiffness matrices, i.e. $Z = \boldsymbol{H}^{-1}$, wherein $\boldsymbol{H}$ represents the FRF matrix. $\boldsymbol{f}$ has the same structure as $\boldsymbol{u}$, and represents the external force vectors at the corresponding DoFs in the (dis)assembled configurations of each (sub)system. The vector $\boldsymbol{g}$, like $\boldsymbol{f}$ represents the disconnection forces felt from the (de)coupling of the adjacent subsystems. Each of the vectors within the set of $\boldsymbol{u}$ represents the displacements in each of the principal x, y, z directions, and $\boldsymbol{f}$ and $\boldsymbol{g}$ represent the forces in these principal directions. Explicit direction and frequency dependency of terms in Eqs. (1–2) are omitted for clarity.

When in contact, connected interface DoFs at matching coupling pairs must have the same displacements, i.e.:

$$\boldsymbol{u}_C^{AB_1} = \boldsymbol{u}_C^{B_1}. \tag{3}$$

Eq. (3) assumes rigid contact. In reality, these joints will have their own flexibilities, which with brevity are presently ignored. The compatibility conditions of Eq. (3) can be rewritten compactly using a Boolean matrix description as:

$$\boldsymbol{B}\boldsymbol{u} = \begin{bmatrix} \boldsymbol{B}^{AB_1} & \boldsymbol{B}^{B_1} \end{bmatrix} \begin{Bmatrix} \boldsymbol{u}^{AB_1} \\ \boldsymbol{u}_C^{B_1} \end{Bmatrix} = \begin{bmatrix} 0 & \boldsymbol{I} & -\boldsymbol{I} \end{bmatrix} \begin{Bmatrix} \boldsymbol{u}^{AB_1} \\ \boldsymbol{u}_C^{B_1} \end{Bmatrix} = \boldsymbol{u}_C^{AB_1} - \boldsymbol{u}_C^{B_1} = 0 \tag{4}$$

wherein $\boldsymbol{B}$ extracts the coupling DoFs from among the full set of DoFs. Formulations presented here are for the 'standard decoupling' case [17], which requires that compatibility and equilibrium be satisfied only at the interface DoFs between subsystem B_1 and the assembled system AB_1.

Equilibrium conditions for an external force $\boldsymbol{f}_A^{AB_1}$ applied at $\boldsymbol{u}_A^{AB_1}$ results in interface forces that balance each other, i.e.:

$$\boldsymbol{g}_C^{AB_1} + \boldsymbol{g}_C^{B_1} = 0. \tag{5}$$

Rewriting the equilibrium conditions in Eq. (5) with a Boolean matrix, we get:

$$\boldsymbol{L}^T\boldsymbol{g} = \begin{bmatrix} \boldsymbol{L}^{AB_1{}^T} & \boldsymbol{L}^{B_1{}^T} \end{bmatrix} \begin{Bmatrix} \boldsymbol{g}^{AB_1} \\ \boldsymbol{g}_C^{B_1} \end{Bmatrix} = 0 \tag{6}$$

wherein $\boldsymbol{L}$ actually represents the nullspace of $\boldsymbol{B}$ or vice versa i.e. $\boldsymbol{L} = \text{null}(\boldsymbol{B})$, or $\boldsymbol{B}^T = \text{null}\left(\boldsymbol{L}^T\right)$ [17].

Employing the dual formulation for decoupling [17], the interface forces are satisfied a priori by choosing the interface forces of the form of:

$$\boldsymbol{g} = \boldsymbol{B}^T\lambda \tag{7}$$

wherein λ are Lagrange multipliers, corresponding physically to the interface force intensities. The equilibrium conditions in Eq. (6) thus become:

$$\boldsymbol{L}^T\boldsymbol{g} = \boldsymbol{L}^T\boldsymbol{B}^T\lambda = 0. \tag{8}$$

Substituting Eq. (8) in Eqs. (1–2) while also accounting for the

compatibility conditions of Eq. (4), the union between the assembled system AB_1 and the subsystem B_1 can be written in compact matrix form as:

$$\begin{bmatrix} \boldsymbol{Z}^{AB_1} & 0 & \boldsymbol{B}^{AB_1{}^T} \\ 0 & -\boldsymbol{Z}^{B_1} & \boldsymbol{B}^{B_1{}^T} \\ \boldsymbol{B}^{AB_1} & \boldsymbol{B}^{B_1} & 0 \end{bmatrix} \begin{Bmatrix} \boldsymbol{u}^{AB_1} \\ \boldsymbol{u}_C^{B_1} \\ \lambda \end{Bmatrix} = \begin{Bmatrix} \boldsymbol{f}^{AB_1} \\ -\boldsymbol{f}_C^{B_1} \\ 0 \end{Bmatrix}. \tag{9}$$

Eq. (9) shows that the decoupling problem is equivalent to assembly of a negative dynamic stiffness for the substructure that one wants to subtract. The decoupled response of subsystem A can be obtained from Eq. (9) by eliminating λ, and by introducing FRF matrices $\boldsymbol{H}^{AB_1}$ and $\boldsymbol{H}^{B_1}$ in place of the dynamic stiffness matrices $\boldsymbol{Z}^{AB_1-1}$ and $\boldsymbol{Z}^{B_1-1}$[17,18]:

$$\begin{aligned} \left[\boldsymbol{H}^{A}\right] = & \begin{bmatrix} \boldsymbol{H}^{AB_1} & 0 \\ 0 & -\boldsymbol{H}^{B_1} \end{bmatrix} - \begin{bmatrix} \boldsymbol{H}^{AB_1} & 0 \\ 0 & -\boldsymbol{H}^{B_1} \end{bmatrix} \begin{bmatrix} \boldsymbol{B}^{AB_1{}^T} \\ \boldsymbol{B}^{B_1{}^T} \end{bmatrix} \\ & \left(\begin{bmatrix} \boldsymbol{B}^{AB_1} & \boldsymbol{B}^{B_1} \end{bmatrix} \begin{bmatrix} \boldsymbol{H}^{AB_1} & 0 \\ 0 & -\boldsymbol{H}^{B_1} \end{bmatrix} \begin{bmatrix} \boldsymbol{B}^{AB_1{}^T} \\ \boldsymbol{B}^{B_1{}^T} \end{bmatrix} \right)^{-1} \\ & \begin{bmatrix} \boldsymbol{B}^{AB_1} & \boldsymbol{B}^{B_1} \end{bmatrix} \begin{bmatrix} \boldsymbol{H}^{AB_1} & 0 \\ 0 & -\boldsymbol{H}^{B_1} \end{bmatrix} \end{aligned} \tag{10}$$

wherein

$$\left[\boldsymbol{H}^{AB_1}\right] = \begin{bmatrix} \boldsymbol{H}_{11}^{AB_1} & \boldsymbol{H}_{12A}^{AB_1} & \boldsymbol{H}_{12B}^{AB_1} & \boldsymbol{H}_{12C}^{AB_1} & \boldsymbol{H}_{12D}^{AB_1} & \boldsymbol{H}_{12E}^{AB_1} \\ & \boldsymbol{H}_{2A2A}^{AB_1} & \boldsymbol{H}_{2A2B}^{AB_1} & \boldsymbol{H}_{2A2C}^{AB_1} & \boldsymbol{H}_{2A2D}^{AB_1} & \boldsymbol{H}_{2A2E}^{AB_1} \\ & & \boldsymbol{H}_{2B2B}^{AB_1} & \boldsymbol{H}_{2B2C}^{AB_1} & \boldsymbol{H}_{2B2D}^{AB_1} & \boldsymbol{H}_{2B2E}^{AB_1} \\ & & & \boldsymbol{H}_{2C2C}^{AB_1} & \boldsymbol{H}_{2C2D}^{AB_1} & \boldsymbol{H}_{2C2E}^{AB_1} \\ & sym & & & \boldsymbol{H}_{2D2D}^{AB_1} & \boldsymbol{H}_{2D2E}^{AB_1} \\ & & & & & \boldsymbol{H}_{2E2E}^{AB_1} \end{bmatrix} \tag{11}$$

wherein $\boldsymbol{H}_{11}^{AB_1}$ corresponds to the tool point receptance matrix, i.e. at location $\boldsymbol{u}_A^{AB_1}$; $\boldsymbol{H}_{12A}^{AB_1}$ … $\boldsymbol{H}_{12E}^{AB_1}$ correspond to the cross receptance matrices between the tool point and each of the five different coupling locations. All other receptance matrices in Eq. (11) correspond to direct and cross receptance matrices between all of the five different coupling locations in the assembled configuration.

Similarly, $\boldsymbol{H}^{B_1}$ within Eq. (10) consists of the direct and cross receptance matrices between all of the five different coupling locations for only the residual subsystem B_1:

$$\left[\boldsymbol{H}^{B_1}\right] = \begin{bmatrix} \boldsymbol{H}_{2A2A}^{B_1} & \boldsymbol{H}_{2A2B}^{B_1} & \boldsymbol{H}_{2A2C}^{B_1} & \boldsymbol{H}_{2A2D}^{B_1} & \boldsymbol{H}_{2A2E}^{B_1} \\ & \boldsymbol{H}_{2B2B}^{B_1} & \boldsymbol{H}_{2B2C}^{B_1} & \boldsymbol{H}_{2B2D}^{B_1} & \boldsymbol{H}_{2B2E}^{B_1} \\ & & \boldsymbol{H}_{2C2C}^{B_1} & \boldsymbol{H}_{2C2D}^{B_1} & \boldsymbol{H}_{2C2E}^{B_1} \\ & sym & & \boldsymbol{H}_{2D2D}^{B_1} & \boldsymbol{H}_{2D2E}^{B_1} \\ & & & & \boldsymbol{H}_{2E2E}^{B_1} \end{bmatrix}. \tag{12}$$

Each of the receptance matrices within Eqs. (10–12) can be represented by direct and cross receptances in each of the principal axis as:

$$\boldsymbol{H} = \begin{bmatrix} h_{xx} & h_{xy} & h_{xz} \\ & h_{yy} & h_{yz} \\ sym & & h_{zz} \end{bmatrix}. \tag{13}$$

All receptances matrices in Eqs. (10–13) are symmetric, assuming reciprocity. Receptance matrices in Eqs. (10–13) neglect the rotational FRFs, especially since experimental estimation of rotational FRFs is complicated and non-trivial. Moreover, since the effect of rotational DoFs is already embedded in each measured FRF of the assembled system [19], ignoring the rotational FRFs may not adversely affect decoupling.

Extracted mobile machine tool dynamics from Eq. (10), i.e. for subsystem A can now be coupled to other base/parts using the substructure coupling technique.

2.2. Substructure coupling

As in the case of substructure decoupling, the equations of motion of the subsystems to be coupled can also be described using the dynamic stiffness representation as:

$$\boldsymbol{Z}\boldsymbol{u} = \boldsymbol{f} + \boldsymbol{g};\ \text{i.e.} \begin{bmatrix} \boldsymbol{Z}^{A} & 0 \\ 0 & \boldsymbol{Z}^{B_2} \end{bmatrix} \begin{Bmatrix} \boldsymbol{u}^{A} \\ \boldsymbol{u}_C^{B_2} \end{Bmatrix} = \begin{Bmatrix} \boldsymbol{f}^{A} \\ \boldsymbol{f}_C^{B_2} \end{Bmatrix} + \begin{Bmatrix} \boldsymbol{g}^{A} \\ \boldsymbol{g}_C^{B_2} \end{Bmatrix} \tag{14}$$

wherein subscripts C and A denote coupling and tool point locations/DoFs respectively. Superscripts A and B_2 denote the subsystems for the machine and the new base respectively. Descriptions for $\boldsymbol{Z}$, $\boldsymbol{f}$, and $\boldsymbol{g}$ are consistent with those in Section 2.1. $\boldsymbol{u}^A$ represents the vector of DoFs corresponding to the tool point and the coupling locations, i.e. $\boldsymbol{u}^A = \left\{ \boldsymbol{u}_A^A;\ \boldsymbol{u}_C^A \right\}^T$. $\boldsymbol{u}_A^A$ is the vector of DoFs corresponding to the tool point in the disassembled configuration, and $\boldsymbol{u}_C^A$ corresponds to the coupling DoFs of the extracted subsystem A, and is composed of the vector of DoFs at all of the five coupling locations, i.e. $\boldsymbol{u}_C^A = \left\{ \boldsymbol{u}_{C_{2A}}^A;\ \boldsymbol{u}_{C_{2B}}^A;\ \boldsymbol{u}_{C_{2C}}^A;\ \boldsymbol{u}_{C_{2D}}^A;\ \boldsymbol{u}_{C_{2E}}^A \right\}^T$. $\boldsymbol{u}_C^{B_2}$ consists of the vector of DoFs for the subsystem B_2 that has only three coupling locations, i.e. $\boldsymbol{u}_C^{B_2} = \left\{ \boldsymbol{u}_{C_{2A}}^{B_2};\ \boldsymbol{u}_{C_{2B}}^{B_2};\ \boldsymbol{u}_{C_{2C}}^{B_2} \right\}^T$.

For coupling, the compatibility condition at the interface DoFs dictate that the three pairs of matching DoFs must have the same displacement, i.e.:

$$\boldsymbol{u}_C^{A*} = \boldsymbol{u}_C^{B_2} \tag{15}$$

wherein $\boldsymbol{u}_C^{A*}$ is a subset of $\boldsymbol{u}_C^A$, i.e. $\boldsymbol{u}_C^{A*} \subseteq \boldsymbol{u}_C^A$, and consists of only the vector of DoFs that are being coupled at the interface to subsystem B_2, i.e. $\boldsymbol{u}_C^{A*} = \left\{ \boldsymbol{u}_{C_{2A}}^A;\ \boldsymbol{u}_{C_{2B}}^A;\ \boldsymbol{u}_{C_{2C}}^A \right\}^T$. Eq. (15) also assumes rigid coupling, neglecting the influence of flexibilities at the connection locations. As before, these compatibility conditions in Eq. (15) can be rewritten compactly using a Boolean matrix description as:

$$\boldsymbol{B}\boldsymbol{u} = \begin{bmatrix} \boldsymbol{B}^A & \boldsymbol{B}^{B_2} \end{bmatrix} \begin{Bmatrix} \boldsymbol{u}^A \\ \boldsymbol{u}^{B_2} \end{Bmatrix} = \begin{bmatrix} 0 & \boldsymbol{I} & -\boldsymbol{I} \end{bmatrix} \begin{Bmatrix} \boldsymbol{u}^A \\ \boldsymbol{u}^{B_2} \end{Bmatrix} = \boldsymbol{u}_C^{A*} - \boldsymbol{u}_C^{B_2} = 0. \tag{16}$$

Again, as before, i.e. in the decoupling case, the connection forces between subsystems should be in equilibrium, i.e.

$$\boldsymbol{g}_C^{A*} + \boldsymbol{g}_C^{B_2} = 0 \tag{17}$$

wherein $\boldsymbol{g}_C^{A*}$ is also a subset of $\boldsymbol{g}_C^A$, i.e. $\boldsymbol{g}_C^{A*} \subseteq \boldsymbol{g}_C^A$. Rewriting the equilibrium conditions also with a Boolean matrix, we get:

$$\boldsymbol{L}^T\boldsymbol{g} = \begin{bmatrix} \boldsymbol{L}^{A^T} & \boldsymbol{L}^{B_2{}^T} \end{bmatrix} \begin{Bmatrix} \boldsymbol{g}^A \\ \boldsymbol{g}_C^{B_2} \end{Bmatrix} = 0. \tag{18}$$

Employing again the dual formulation for coupling [7], the interface forces take the same form as in Eq. (7). The equilibrium forces also take the general form of Eq. (8). Substituting the modified form of Eq. (8) in Eq. (14) and also accounting for the compatibility conditions of Eq. (16), the union between the subsystems A and AB_2 can be written in compact matrix form as:

$$\begin{bmatrix} \boldsymbol{Z}^A & 0 & \boldsymbol{B}^{A^T} \\ 0 & \boldsymbol{Z}^{B_2} & \boldsymbol{B}^{B_2{}^T} \\ \boldsymbol{B}^A & \boldsymbol{B}^{B_2} & 0 \end{bmatrix} \begin{Bmatrix} \boldsymbol{u}^A \\ \boldsymbol{u}_C^{B_2} \\ \lambda \end{Bmatrix} = \begin{Bmatrix} \boldsymbol{f}^A \\ \boldsymbol{f}_C^{B_2} \\ 0 \end{Bmatrix}. \tag{19}$$

Eliminating λ from Eq. (19) and introducing FRF matrices $\boldsymbol{H}^A$ and $\boldsymbol{H}^{B_2}$ in place of the dynamic stiffness matrices $\boldsymbol{Z}^{A-1}$ and $\boldsymbol{Z}^{B_2-1}$, the coupled system response for AB_2 can be shown to be [7,18]:

$$\begin{aligned} \left[\boldsymbol{H}^{AB_2}\right] = & \begin{bmatrix} \boldsymbol{H}^A & 0 \\ 0 & \boldsymbol{H}^{B_2} \end{bmatrix} - \begin{bmatrix} \boldsymbol{H}^A & 0 \\ 0 & \boldsymbol{H}^{B_2} \end{bmatrix} \begin{bmatrix} \boldsymbol{B}^{A^T} \\ \boldsymbol{B}^{B_2{}^T} \end{bmatrix} \\ & \left(\begin{bmatrix} \boldsymbol{B}^A & \boldsymbol{B}^{B_2} \end{bmatrix} \begin{bmatrix} \boldsymbol{H}^A & 0 \\ 0 & \boldsymbol{H}^{B_2} \end{bmatrix} \begin{bmatrix} \boldsymbol{B}^{A^T} \\ \boldsymbol{B}^{B_2{}^T} \end{bmatrix} \right)^{-1} \\ & \begin{bmatrix} \boldsymbol{B}^A & \boldsymbol{B}^{B_2} \end{bmatrix} \begin{bmatrix} \boldsymbol{H}^A & 0 \\ 0 & \boldsymbol{H}^{B_2} \end{bmatrix} \end{aligned} \tag{20}$$

wherein $\boldsymbol{H}^A$ is obtained from Eq. (10), and $\boldsymbol{H}^{B_2}$ consists of the direct and cross receptance matrices between all the three different coupling locations for only the subsystem B_2:

$$\left[\boldsymbol{H}^{B_2}\right] = \begin{bmatrix} \boldsymbol{H}^{B_2}_{2\tilde{A}2A} & \boldsymbol{H}^{B_2}_{2\tilde{A}2B} & \boldsymbol{H}^{B_2}_{2\tilde{A}2C} \\ & \boldsymbol{H}^{B_2}_{2\tilde{B}2B} & \boldsymbol{H}^{B_2}_{2\tilde{B}2C} \\ sym & & \boldsymbol{H}^{B_2}_{2\tilde{C}2C} \end{bmatrix}. \tag{21}$$

Each of the receptance matrices in Eqs. (20–21) also takes the form of Eq. (13). Even though rotational FRFs are thought necessary in the substructure coupling procedures, they are presently neglected; primarily since they are notoriously difficult to measure, and since the extracted FRF matrix for subsystem A also does not contain them. Using the dual formulation for coupling, the rows and columns corresponding to the coupling DoFs appear twice in $\boldsymbol{H}^{AB_2}$, and only independent entries need to be retained.

3. Experimental considerations

Experimental substructuring remains challenging due to issues related to noise in the measured FRFs, inability to measure exact coupling locations on the structure, potential errors due to truncation, and violations of linearity and reciprocity.

Truncation errors, i.e. errors related to unmeasured modes that may exist outside the measured frequency range are avoided by measuring up to 2.5 kHz. This range is thought to be far beyond the highest frequency of interest, with the high-frequency tool modes lying in the 1000–1500 Hz range.

Because of the matrix inversion operations necessary for (de) coupling (see Eqs. (10) and (20)), any noise in the measurements may lead to ill-conditioning and matrix singularity errors [20]. To avoid this, all measured receptances are curve fit to regenerate FRFs from a consistent modal model [21]. As a representative example, the raw measured FRF at the representative coupling point 2D (shown in Figs. 1 and 3) for the assembled system AB_1 is compared with the fitted FRF in Fig. 2 for response in the X_{MT} direction. Even though FRFs were measured up to 2.5 kHz, Fig. 2 limits the comparison up to 1 kHz, since no significant higher frequency modes were observed. As evident, the modal fitted FRF appears more consistent.

Inability to obtain a driving point measurement at the 'true' connection DoF is also a known major source of concern when (de) coupling [20]. Moreover, since each coupling pair can be measured on the machine, or on the base side, FRFs at both locations as shown in Fig. 3(a and b) are measured and compared in Fig. 4. Comparisons in Fig. 4, limited to the X_{MT} direction only, are made

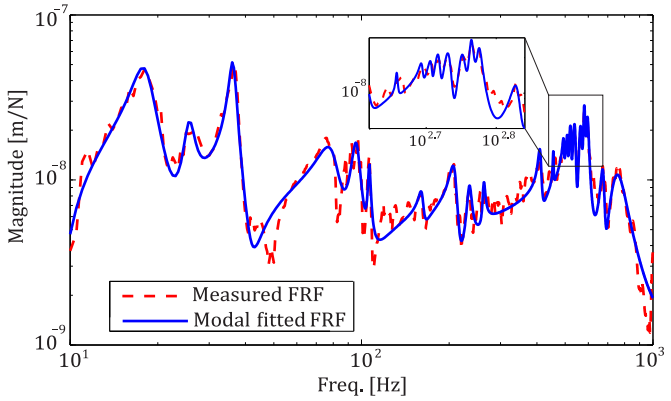

Fig. 2. Comparison of raw measured FRF with modal fitted FRF at the coupling location 2D for system AB_1 in the X_{MT} direction.

for the representative coupling pair 2D, which is one of the five coupling pairs for the assembled system AB_1.

As evident in Fig. 4, though the number of measured modes and the general trend of the measurements is the same, there are slight differences between measurements made at the base side and at the machine side. Low-frequency modes (up to 50 Hz) measured at the base side are dynamically slightly stiffer than at the machine side, whereas the high-frequency modes at the base side are slightly more flexible than the measurements at the machine side. Since either of these points is idealized to represent the 'true' coupling point, influence, if any, of the differences between assuming all of the coupling points to lie on the base side or on the machine side during (de)coupling is treated in Section 4.

Reciprocity checks were carried out and sample comparisons are shown in Fig. 5, which shows measured FRFs between the coupling pairs 2A and 2D for the assembled system AB_1 as shown in Fig. 3(c). Fig. 5 limits comparisons up to 500 Hz since the measured spectrum did not show any significant high-frequency modes. Slight differences in the dynamic stiffness's between these cross FRFs could be attributed to differences in accelerometer placement and excitation locations, issues that lead to controllability and/or observability related errors [7].

4. Substructuring results

Following the substructuring scheme in Section 2.1, at first the mobile machine tool dynamics (subsystem A) are extracted using Eq. (10). These extracted dynamics are subsequently coupled to measured dynamics of subsystem B_2 to predict the assembled AB_2 system dynamics using Eq. (20). These predicted dynamics of AB_2 are compared in Fig. 6 with the measured dynamics for the machine in the assembled AB_2 configuration. Response comparisons in Fig. 6 are limited to the primary location of interest, i.e. at the tool center point (TCP). A cylinder with a diameter of 20 mm is mounted in the tool holder to mimic an end mill with the same diameter.

Response in all three principal directions of the machine is compared across the full frequency range of interest, i.e. up to 1.5 kHz. All FRFs employed in the substructuring scheme (decoupling+coupling) for the results in Fig. 6 are modal fitted prior to substructuring. Influence of employing raw measured FRFs is discussed separately in Fig. 7. Furthermore, the predicted assembled system response in Fig. 6 is for the case of assuming all the 'true' coupling locations to lie on the machine side. Influence of assuming all the 'true' coupling locations to lie on the base side is discussed separately in Fig. 8.

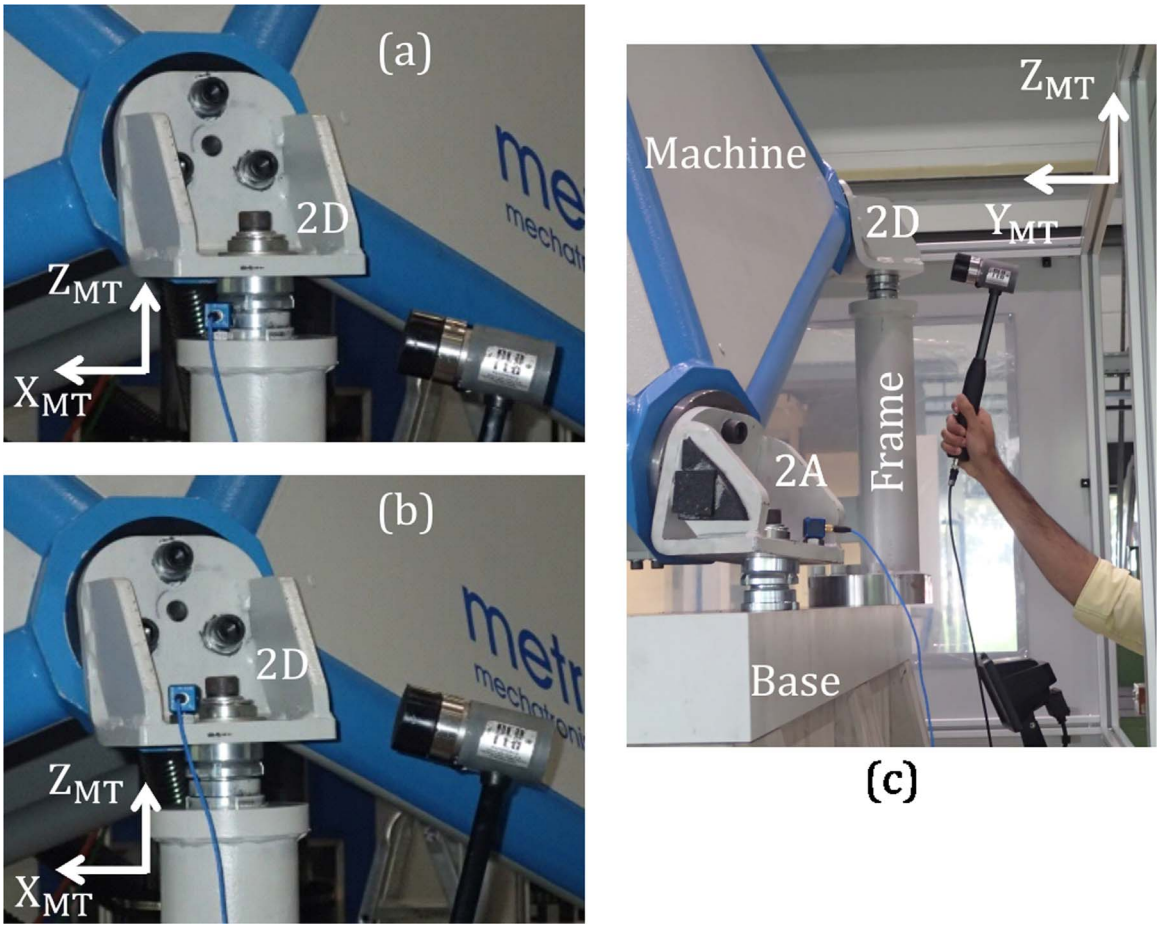

Fig. 3. (a) Approximated driving point at coupling location 2D for system AB_1, measured at the base side (b) Approximated driving point at coupling location 2D for system AB_1, measured at the machine side; (c) Cross FRF measurements between locations 2A and 2D for system AB_1.

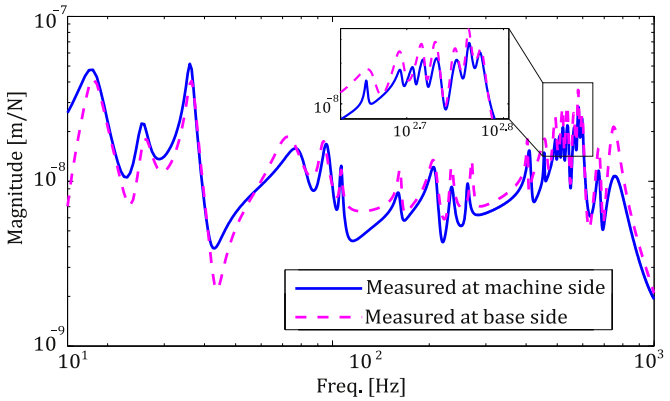

Fig. 4. Comparison of approximated driving point FRFs at coupling location 2D for the assembled system AB_1. FRFs compared between measurements made on machine side and base side.

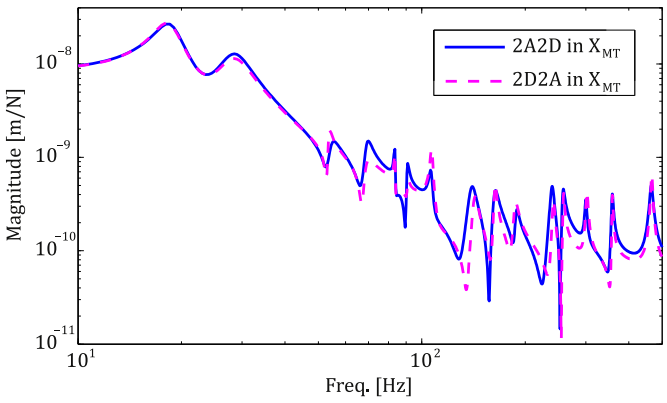

Fig. 5. Reciprocity check for measurements made between locations 2A and 2D for the assembled system AB_1.

As is evident in Fig. 6, the proposed substructuring scheme can approximate the measured trend reasonably well. Dynamic stiffness as observed at the tool point is almost as flexible at the low-frequency as it is at the high-frequency. This peculiarity, specific to the kinematic makeup of this parallel kinematic machine, is captured well by the substructuring scheme.

The differences in Fig. 6 in the low-mid-frequency range are thought to be due to observability/controllability related issues at the points of coupling. If some modes are not excitable and/or are not observable at the points of coupling, these unmeasured modes contribute towards substructuring errors. This may explain the modal mismatch in the Y_{MT} direction (Fig. 6(b)) in the 80–400 Hz range and in the Z_{MT} direction (Fig. 6(c)) in the 30–100 Hz range. Neglecting flexibilities at the coupling interfaces are also thought to contribute to errors in correctly predicting the dynamic stiffness' at the low frequencies. Low coherence in measured FRFs further contributes to errors observed at the low frequencies. Discrepancies may also be attributed to decoupling being sensitive around the anti-resonances of the known subsystem(s), and to coupling being sensitive around the resonances of the subsystems [17]. Local high-frequency modes in the 650–1200 Hz range belonging to the spindle and tool-tool-holder combination are better approximated since these are less affected by observability/

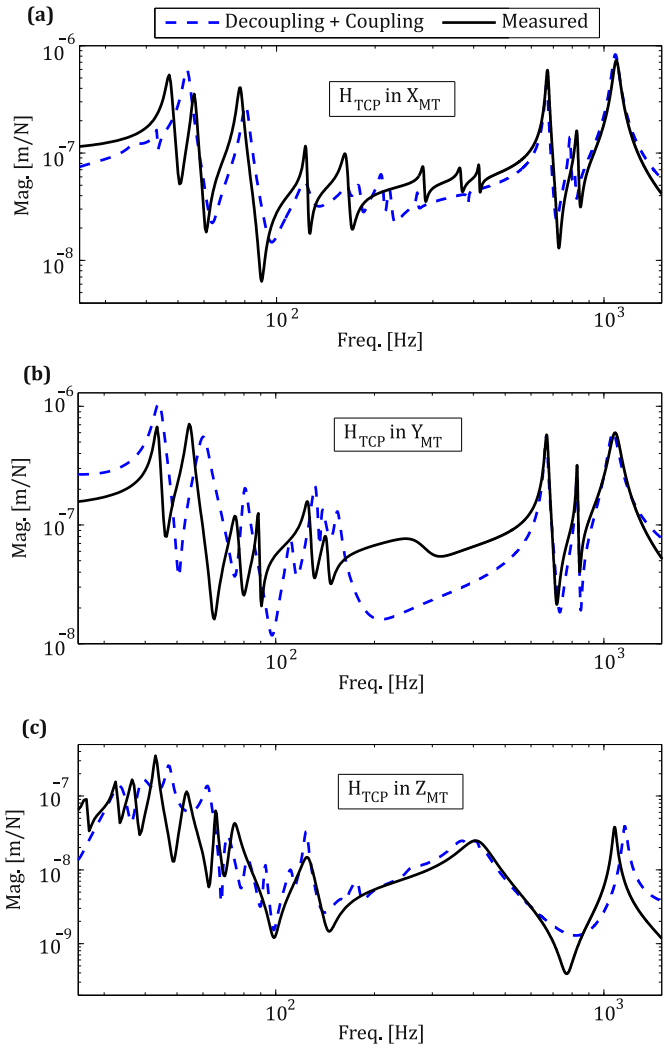

Fig. 6. Comparison of assembled tool point dynamics (FRFs) for system AB_2 predicted via substructuring (i.e. decoupling+coupling) with measured dynamics in the assembled configuration. (a) Results in X_{MT} direction; (b) results in Y_{MT} direction; (c) results in Z_{MT} direction;

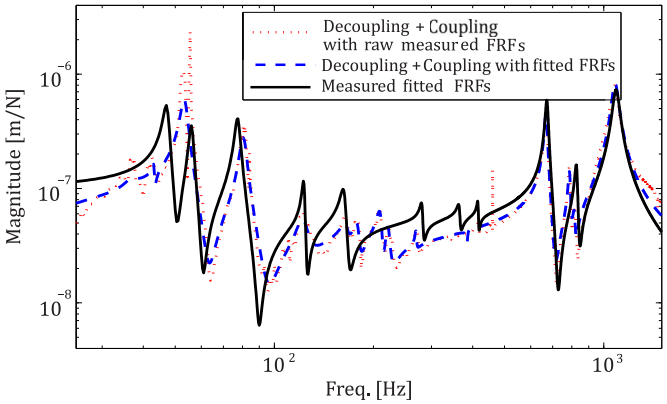

Fig. 7. Results of substructuring with raw measured FRFs as compared with substructuring results with modal fitted FRFs, and measured FRFs. Comparisons limited to assembled tool point location in the X_{MT} direction.

controllability issues at the coupling points. Controllability could potentially be addressed by using a modal shaker that can provide a more consistent impact in place of the modal impact hammer that was presently used. However, the elaborate experimental setup to instrument a shaker is impractical for the present

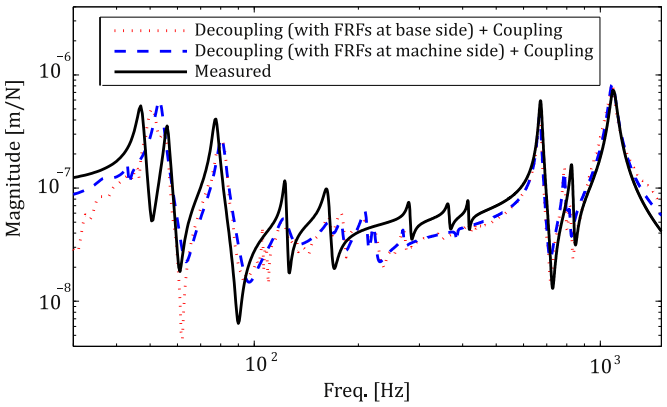

Fig. 8. Comparison of substructuring results as influenced by approximating 'true' coupling locations to lie either on the base or on the machine side during the decoupling procedure. FRFs are shown only at the tool point location in the X_{MT} direction.

application, which relies on quick measurement of FRFs that can be easily measured on site using a modal impact hammer and a set of one or more accelerometers.

Results obtained using raw measured FRFs in the (de)coupling procedure are compared with substructuring results obtained with modal fitted FRFs and measured FRFs in Fig. 7. As evident in Fig. 7, which compares response in only the X_{MT} direction, though the use of raw measured FRFs in the (de)coupling procedures results in some spikes at ~53 Hz and at ~460 Hz, results follow the measured trend quite well. Furthermore, as is evident in Fig. 8, when the 'true' coupling location is assumed to lie on the base, base flexibilities will be part of the extracted machine dynamics. Since the base response is dominated by low-frequency modes, there is some discrepancy in assembled system response between assuming the 'true' coupling location to lie on either the base or the machine side.

Overall, from Figs. 6–8, it is evident that the substructuring procedures employed can adequately approximate dynamics of measured systems. Neglecting the flexibilities at the coupling locations, measurement noise, and approximation of 'true' coupling locations, though were not observed to adversely influence the (de)coupling procedures, need to be investigated further – planned as part of our future work.

5. Conclusions

Prediction of mobile machine tool dynamics prior to moving the machine to any new part and location is essential to guide first-time right in situ machining solutions. This paper, through the use of substructure (de)coupling techniques shows that it is indeed possible to couple the extracted dynamics of the mobile machine tool with measured dynamics of any base/part (measured at location) to predict the assembled system dynamics prior to moving the mobile machine to a new and arbitrary base/part. Using the decoupling scheme, it is shown that it is possible to extract unsupported free–free response of an entire machine tool structural system, something that is non-trivial to do otherwise. Methods presented in the paper use and rely on measured FRFs that are easy enough to obtain, making the methods efficient and easily implementable.

Sensitivity of the extracted machine dynamics to changes in the residual substructural base system needs further experimental characterization. Furthermore, since access to machine tool interfaces are often restricted in their assembled configurations, exploring other decoupling schemes that allow determination of

decoupled dynamics without knowledge of response at the driving points at the interfaces may indeed prove useful. Results obtained in this paper motivate the need for additional research on experimental substructuring in the context of its applications in machine tools. Methods presented could indeed find use in structural joint identification, and in facilitating modularity, mutability and re-configurability of machine tools and its components.

References

[1] L. Uriarte, M. Zatarain, D. Axinte, J. Yagüe-Fabra, S. Ihlenfeldt, J. Eguia, A. Olarra, Machine tools for large parts, CIRP Ann. 62 (2013).

[2] N. Neugebauer, M. Wabner, H. Rentzsch, S. Ihlenfeldt, Structure principles of energy efficient machine tools, CIRP J. Manuf. Sci. Technol. 4 (2011) 136–147.

[3] M. Schwaar, T. Schwaar, S. Ihlenfeldt, H. Rentzsch, Mobile 5-axis machining centres, in: Proceedings of the Chemnitz International Manufacturing Colloquium, 2010.

[4] R.R. Craig Jr, M.C. Bampton, Coupling of substructures for dynamic analyses, AIAA J. 6 (1968) 1313–1319.

[5] M. Zatarian, E. Lejardi, F. Egana, Modular synthesis of machine tools, CIRP Ann. 47 (1998) 333–336.

[6] M. Law, Y. Altintas, A.S. Phani, Rapid evaluation and optimization of machine tools with position-dependent stability, Int. J. Mach. Tools Manuf. 68 (2013) 81–90.

[7] D. de Klerk, D. Rixen, S. Voormeeren, General framework for dynamic substructuring: history, review and classification of techniques, AIAA J. 46 (5) (2008) 1169–1181.

[8] T. Schmitz, R. Donaldson, Predicting high-speed machining dynamics by substructure analysis, CIRP Ann. 49 (2000) 303–308.

[9] S. Park, Y. Altintas, M. Movahhedy, Receptance coupling for end mills, Int. J. Mach. Tools Manuf. 43 (2003) 889–896.

[10] P. Albertelli, M. Goletti, M. Monno, A new receptance coupling substructure analysis methodology to improve chatter free cutting conditions, Int. J. Mach. Tools Manuf. 72 (2013) 16–24.

[11] I. Mancisidor, A. Urkiola, R. Barcena, et al., Receptance coupling for tool point dynamics prediction by fixed boundaries approach, Int. J. Mach. Tools Manuf. 78 (2014) 18–29.

[12] M. Law, S. Ihlenfeldt, A frequency based substructuring approach to efficiently model position-dependent dynamics in machine tools, J. Multi-body Dyn. 229 (2014) 304–317.

[13] C. Brecher, S. Bäumler, M. Daniels, Prediction of dynamics of modified machine tool by experimental substructuring, in: Proceedings of the 32nd IMAC, 2014.

[14] M. Mehrpouya, E. Graham, S. Park, FRF based joint dynamics modeling and identification, Mech. Syst. Signal Process. 39 (2013) 265–279.

[15] M. Law, H. Rentzsch, S. Ihlenfeldt, Development of a dynamic substructuring framework to facilitate in situ machining solutions using mobile machine tools, Procedia Manuf. 1 (2015) 756–767.

[16] M. Law, H. Rentzsch, S. Ihlenfeldt, M. Putz, Application of substructure decoupling techniques to predict mobile machine tool dynamics: numerical investigations, Procedia CIRP 46 (2016) 537–540.

[17] S. Voormeeren, D. Rixen, A family of substructure decoupling techniques based on dual assembly approach, Mech. Syst. Signal Process. 27 (2012) 379–396.

[18] W. D'Ambrogio, A. Frefolent, The role of interface DoFs in decoupling of substructures based on the dual domain decomposition, Mech. Syst. Signal Process. 24 (2010) 2035–2048.

[19] W. D'Ambrogio, A. Frefolent, Are rotational DoFs essential in substructure decoupling?, in: Proceedings of the 32nd IMAC, 2014.

[20] D. Nicgorski, P. Avitabile, Experimental issues related to frequency response function measurements for frequency-based substructuring, Mech. Syst. Signal Process. 24 (2010) 1324–1337.

[21] D. Ewins, Modal Testing: Theory, Practice, and Application, 2nd ed., Taylor & Francis, London, 2000.